applied sciences

MDPI

Article

An On-Chip Silicon Photonics Thermometer with Milli-Kelvin Resolution

Jin Wang [1], Yijie Pan [1,*], Jianxin Gao [2], Cheng Zhang [3], Zhier Qu [3], Tongtong Xu [3], Yang Shen [2] and Jifeng Qu [1,*]

[1] Center for Advanced Measurement Science, National Institute of Metrology, Beijing 100029, China; wangjin@nim.ac.cn
[2] College of Optical and Electronic Technology, China Jiliang University, Hangzhou 310018, China; jxgao195@163.com (J.G.); yshen@cjlu.edu.cn (Y.S.)
[3] School of Optics and Photonics, Beijing Institution of Technology, Beijing 100081, China; 3120205336@bit.edu.cn (C.Z.); 3220200451@bit.edu.cn (Z.Q.); 3220190439@bit.edu.cn (T.X.)
* Correspondence: panyijie@nim.ac.cn (Y.P.); qujifeng@nim.ac.cn (J.Q.)

Abstract: Photonic-based thermometers have been attracting intense research interest as a potential alternative to traditional electrical thermometers due to their physical and chemical stability and immunity to electromagnetic interference. However, due to the high requirements for the stability of the laser source, the existing studies on resolution are only theoretical predictions and do not include real-measured results. In this paper, we report on the fabrication and characterization of an on-chip silicon whispering-gallery-mode (WGM) ring resonator thermometer. The strip grating and the ring structure were fabricated on the silicon-on-insulator (SOI) substrate by two-step etching. The quality-factor (Q-factor), temperature sensitivity, and measurement range of the packaged device were 21,400, 42 pm/K, and 150 K, respectively. The real-measured temperature resolution of 2.9 mK was achieved by virtue of the power and polarization stabilization of the laser source.

Keywords: photonic thermometer; WGM resonator; fabrication technologies

Citation: Wang, J.; Pan, Y.; Gao, J.; Zhang, C.; Qu, Z.; Xu, T.; Shen, Y.; Qu, J. An On-Chip Silicon Photonics Thermometer with Milli-Kelvin Resolution. *Appl. Sci.* **2022**, *12*, 3713. https://doi.org/10.3390/app12083713

Academic Editor: Andreas Fischer

Received: 25 February 2022
Accepted: 3 April 2022
Published: 7 April 2022

1. Introduction

The ability to measure temperature with high resolution is significantly in demand in various fields of industrial production and scientific research, such as biomedicine monitoring [1–3], fabrication process control [4], ecological environmental monitoring [5], etc. Until now, the most widely used thermometers have been based on electrical methods, such as resistance measurement [6] or the Seebeck effect [7]. Although electrical thermometers can provide satisfying temperature measurement results, their chemical instability and sensitivity to mechanical shock induce resistance drift and, furthermore, systematic error, thus requiring frequent calibrations [8–10]. In addition, electrical thermometers are susceptible to electromagnetic interference, thereby limiting their application scenarios.

In contrast, photonic thermometers that feature physical and chemical stability and immunity to electromagnetic interference have become a hot topic for research [11–14]. Among the various kinds of photonics thermometers, WGM resonators have a compelling application potential due to their advantages, including a high detection resolution and a low fabrication difficulty [15–17]. Kim et al. first reported WGM resonators used for thermometry; the authors proved that mode shifting based on the thermo-optic effect could be used for temperature sensing, and the response time was less than 6 µs [14]. Since then, many groups have made efforts to optimize WGM resonator thermometers in terms of temperature measurement range, sensitivity, and resolution. Xiao and Dong's research groups proposed a method to improve the temperature measuring sensitivity by coating the surface of the resonator with organic materials to change the effective thermal-refractive coefficient [18,19]. Ahmed et al. extended the concepts explored by Kim et al., optimizing the device geometry [20] and predicting the theoretical limit of the resolution to

be 80 μK [15]. Furthermore, Ahmed et al. studied the issue of interchangeability in the mass production process [21] and the performance stability of silicon photonic thermometers in environments with strong radiation [22]. Yu et al. [23] applied the Vernier effect induced by a cascaded ring resonator to improve the temperature measurement range and sensitivity. Janz et al. [24] and Yang et al. [25] adopted pattern recognition and barcode methods, expanding the temperature range to exceed the limit of free-space-range (FSR). Liu et al. [26] and Gu et al. [27] utilized ring resonators for cryogenic temperature and dew point sensing, respectively. Pan et al. studied the improvement of resolution [17] and the systematic error induced by self-heating [28]. Nevertheless, the research on resolution has remained only in the realm of theoretical evaluation, and there are no reports of real-measured results.

In this paper, an on-chip silicon WGM ring resonator thermometer is demonstrated, and a real-measured temperature resolution of 2.9 mK is achieved. The device structure and fabrication details are provided, and the related parameters of the device, such as the Q-factor, temperature sensitivity, and measuring range, are measured. In addition, a temperature resolution measuring system is proposed. Finally, using a PT100 temperature sensor as a measurement reference, the resolution of the thermometry system is improved by adjusting the power and polarization stability of the laser source.

2. Materials and Methods

The fabrication processing flow of the device is illustrated in Figure 1. The standard 1-mm-thick SOI wafer contains a Si substrate, a SiO_2 layer with a thickness of 500 nm, and a 220-nm-thick Si top with a crystal orientation of <100> direction. After cleaning the surface with acetone, ethanol, and deionized water in turn, the surface was uniformly coated with polymethyl methacrylate (PMMA) as the photoresist and etching mask. Next, the electron-beam-lithography (EBL: JEOL, JBX-8100) and inductive coupled plasma (ICP: Oxford PlasmaPro 100) etching were implemented for the pattern that forms the ring resonator and the waveguide structure; the etching depth was 220 nm (Figure 1b). Next, the above process was repeated, but the pattern used was for the grating structure, and the etching depth was 70 nm (Figure 1c). Therefore, light can couple into the waveguide and travel around the ring resonator, as shown in Figure 1d.

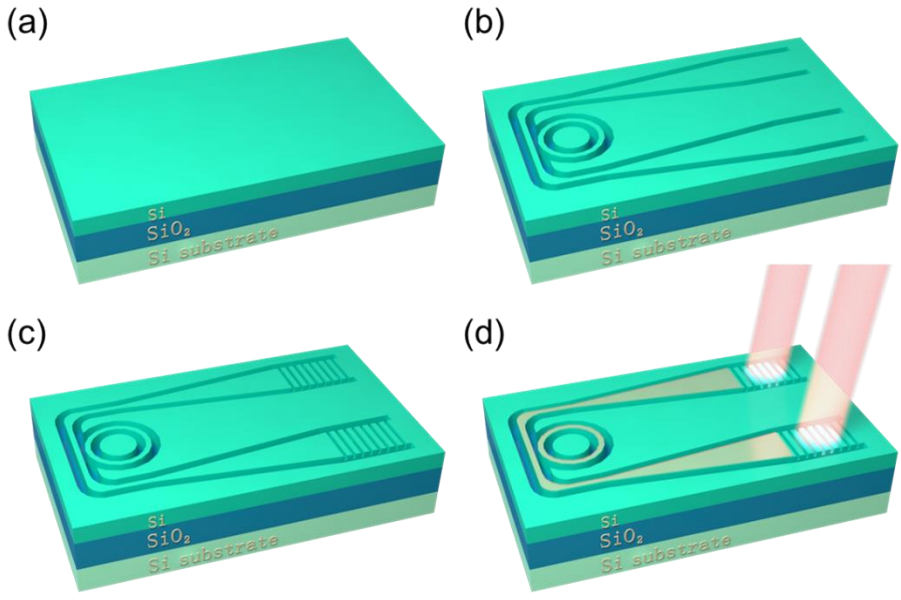

Figure 1. Fabrication process of the device. (**a**) A standard SOI substrate; (**b**) waveguide and resonator etching; (**c**) grating etching; (**d**) optical path diagram.

The packaged device structure of the on-chip silicon WGM ring resonator thermometer is shown in Figure 2a. The chip is stuck to a fiber terminal with UV-curing optical adhesives. The light from the probe laser travels between the fiber and waveguide in the chip through

the strip grating (Figure 2b). From the scanning electron microscope (SEM) image of the micro-morphology shown in Figure 2c,d, the sidewall of the ring resonator is vertical and smooth, reducing scattering loss and thus improving the confinement of the optical field. The width and depth of the waveguide and ring resonator are 500 and 220 nm, respectively, ensuring single-mode transmission [29]. The gap between them is 90 nm in order to obtain a relatively high coupling efficiency. The radius of the ring resonator is 10 µm. The geometric parameters of the grating structure were optimized by a finite-difference-time-domain (FDTD) simulation of coupling efficiency. On the condition that the laser incidence angle is 8° and the grating fill-factor is 0.5, the effects of various etching depths and grating periods on the coupling efficiency are simulated, as shown in Figure 3. When the grating period and etching depth are 615 and 70 nm, respectively, the coupling efficiency at a wavelength of 1550 nm can achieve 47%, which is enough for detection. A detailed description of the grating structure can be found in [30].

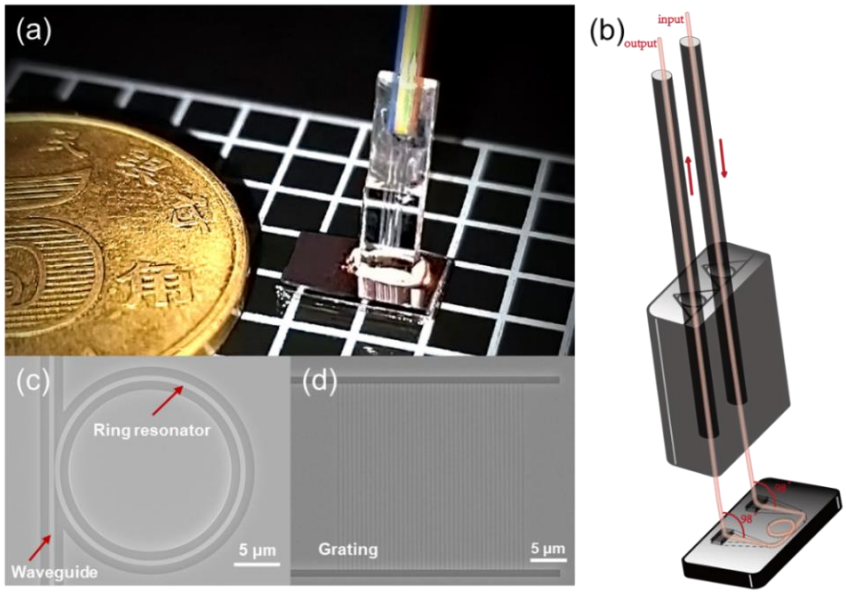

Figure 2. (**a**) An artistically enhanced photo of the packaged device. (**b**) Diagram of the device structure and laser path. SEM images of (**c**) the resonator and (**d**) grating area.

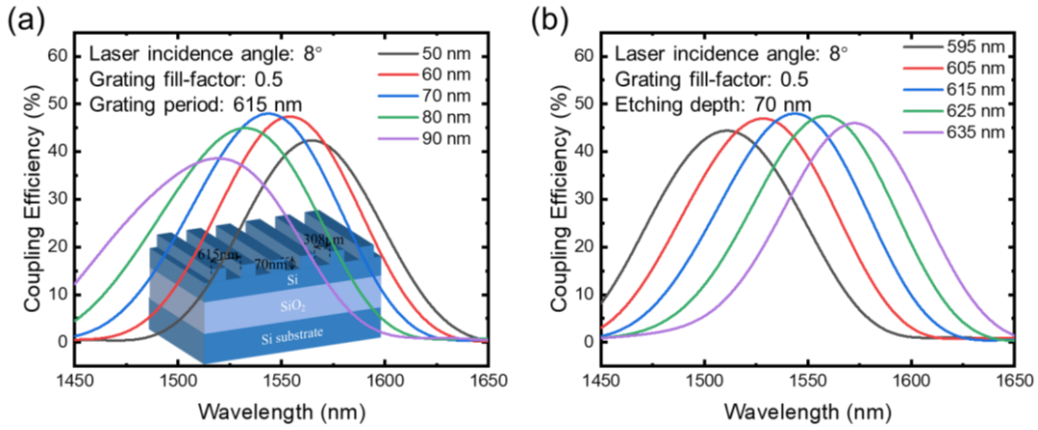

Figure 3. The coupling efficiency as a function of the wavelength of the probe laser source. The comparison of various (**a**) etching depths and (**b**) grating periods. The inset in figure (**a**) shows the schematic and geometric parameters of the optimized structure.

Figure 4 shows the schematic of the experimental measurement setup. The emitted light from the laser was separated into two paths by splitter-1. 90% of the light was

modulated by an acousto-optic modulator (AOM) and then passed through an in-line polarizer and splitter-2. Afterwards, 10% of the light was directed into a photodetector (PD), thus converting the optical power into voltage. A proportional–integral (PI) controller was used to maintain the PD voltage at a fixed value, and the feedback signal was input to the radio frequency (RF) source for amplitude modulation. Because there is a positive correlation between the optical power of the light passing through the AOM and the amplitude of the RF signal applied to the AOM, the feedback loop (the part marked by a green background in Figure 4) can stabilize the output laser power. The in-line polarizer in the feedback loop was used to guarantee the uniform polarization of the output light, which is necessary for resonator transmission spectra detection. The amplitude modulation of the AOM induces a change in polarization of the output light, and the coupling efficiency of the grating structure is selective for polarization; therefore, polarization stabilization can avoid unnecessary fluctuations in the power of the transmitted laser. The packaged device was immersed in a silicone oil bath with adjustable temperature, together with a Pt100 temperature sensor for comparison. Because this method required the laser output frequency to be locked on the side of fringe of the transmission mode, 10% of the light after splitter-1 was sent into a wavemeter (WM) to measure the wavelength, and we utilized a proportional-integral-derivate (PID) feedback signal to control the tunable semiconductor laser, maintaining the wavelength at a fixed value.

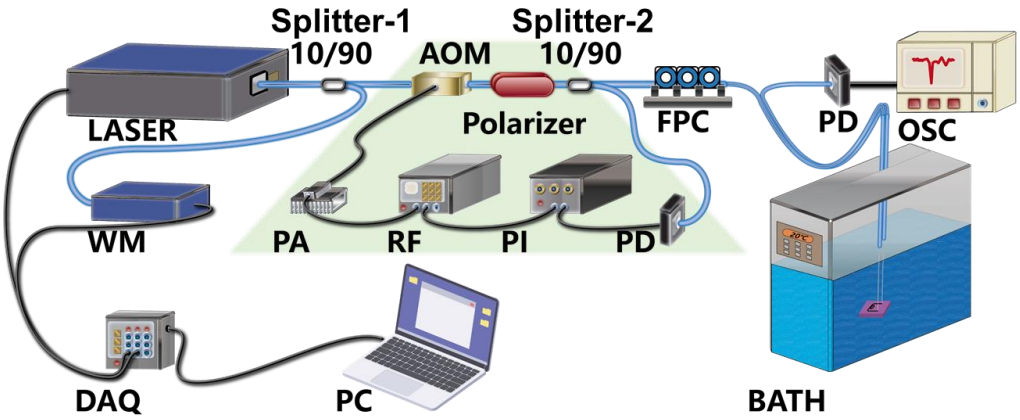

Figure 4. Diagram of experimental setup for device performance characterization. Blue lines represent optical paths, and black lines represent electrical paths. Laser: Toptica, CTL1550; WM (wavemeter): High Finesse, WSU10-IR2; DAQ (data acquisition card): National Instrument, USB-6361; PA (power amplifier): Mini-circuits, ZHL-1-2W-S+; AOM: AA opto-electronic, MT200-IIR30-Fio; RF: Rigol, DSG815; PI: New Focus, LB1005; Polarizer: Thorlabs, ILP1550PM-APC; PD: Thorlabs, PDA20CS-EC; FPC (fiber polarization controllers): Thorlabs, FPC032; Bath: Fluke, 7341; OSC (oscilloscope): Keysight DSOX3054T.

3. Results and Discussion

The performance of the ring resonator thermometer is shown in Figure 5. The probe laser scanned the wavelength around 1550 nm, and the transmission spectrum was obtained. Figure 5a shows the transmission of an unpackaged device. The overall envelope shows a maximum value at a wavelength of around 1545 nm, close to the expected value in Figure 3. The power ratio of transmitted light to incident light is 9.73%, indicating a single coupling efficiency of 31.13%, below the simulated value; this may be due to the difference between the real geometric structure and the designed parameters as well as due to material absorption loss. The full-width-at-half-maximum (FWHM) of resonating mode is 0.021 nm as measured in an atmospheric environment, indicating a Q-factor of 73,400. After the packaging, the transmission is as shown in Figure 5b: the Q-factor dropped to 21,400, and the FSR is reduced from 8.64 to 6.59 nm, which results from the fact that the adhesives change the refractive index environment around the resonator.

When the environment temperature changes, the peak wavelength of resonating mode shifts, approximately following the equation:

$$\Delta\lambda = \frac{\lambda\Delta T}{n_g}\left(\frac{\partial n_{eff}}{\partial T} + \frac{n_{eff}}{L}\frac{\partial L}{\partial T}\right), \quad (1)$$

where λ, $\Delta\lambda$, T, ΔT, n_g, n_{eff}, and L are wavelength, wavelength variation, temperature, temperature variation, group index, effective refractive index, and ring perimeter, respectively. Given that the thermal expansion coefficient of silicon (3.57×10^{-6}/K) is two orders of magnitude smaller than the thermo-optic coefficient (2×10^{-4}/K), an environment temperature change has a negligible impact on the result. The wavelength shifting from −30 to 120 K does not exceed the FSR (Figure 5c), indicating a temperature range over 150 K with a sensitivity of 42 pm/K (Figure 5d). It should be pointed out that the reason why this sensitivity is quite different from the values previously reported (~70 pm/K) is that the adhesives change the effective thermo-optic coefficient, similar to the effect reported in [23].

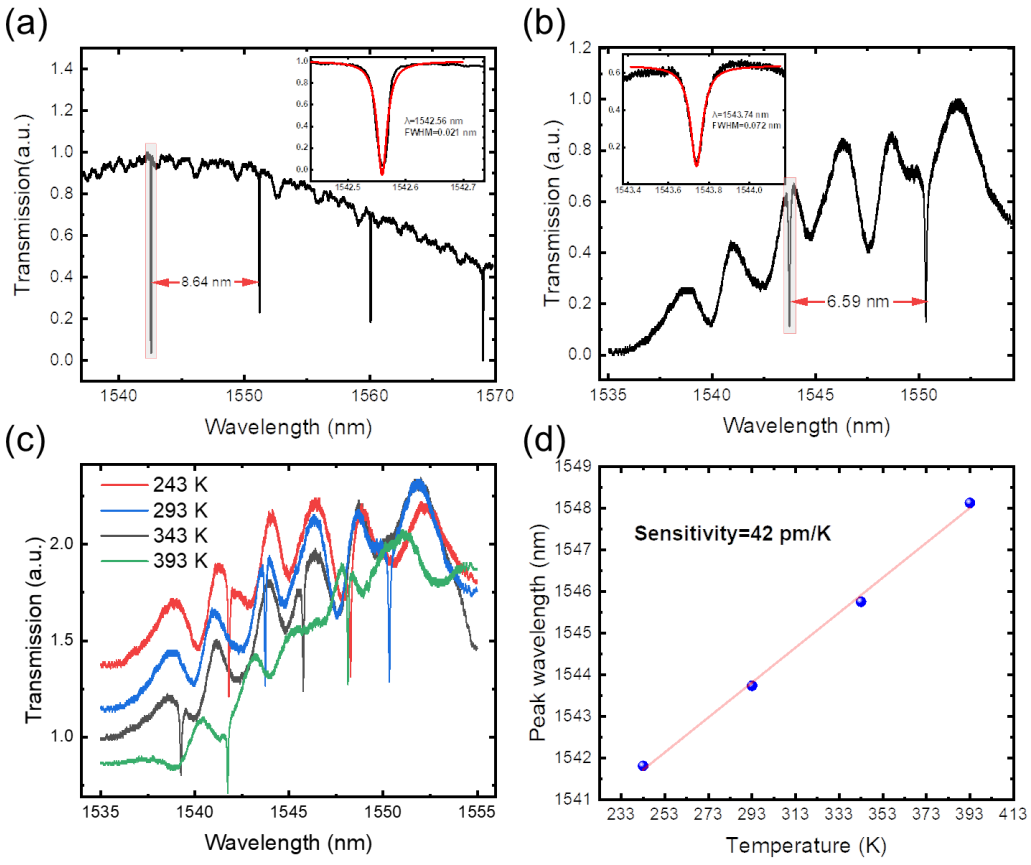

Figure 5. The transmission spectrum of (**a**) unpackaged device and (**b**) packaged device. (**c**) The transmission spectra under various temperatures. (**d**) Peak wavelength of resonating mode versus various temperatures.

The above wavelength scanning method is suitable for the measurement of a relatively wide temperature range, but for a small temperature change (<1 K), the wavelength locking method should be applied, where the wavelength of the laser source is locked at the blue detuning fringe of the resonating mode, and the power of the transmission laser is recorded to represent the small temperature change. This method requires a high stability for both the power and polarization of the laser source. Figure 6a shows the results of the power stabilization; the relative fluctuations over a period of 20 min are reduced from 5‰ (red line) to 2‰ (blue line) after implementing the power stabilization. In order to show the

effect of the polarization stabilization, the output laser from the feedback loop is given access to an additional polarizer, and then the power is recorded under two conditions: with and without polarizers in the loop, as shown in Figure 6b. The in-loop polarizer significantly reduces the relative fluctuations from 57.2 ‰ (red line) to 1.18‰ (blue line).

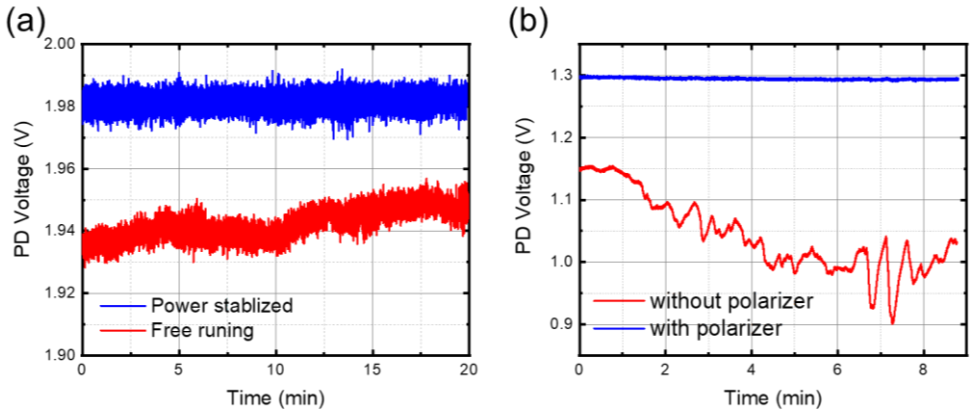

Figure 6. Comparison of (**a**) power and (**b**) polarization stability with or without feedback control.

After the wavelength locking and stabilization of the laser source, the power stability of the transmission laser is as shown in Figure 7a. The standard deviation of the equivalent temperature fluctuation is 2.9 mK, with an actual environment temperature fluctuation of less than 1 mK (measured by the Pt100 temperature sensor), representing the measurement resolution of this thermometer. Figure 7b shows the behavior of the wavelength locking method. The black line is measured by the Pt100 temperature sensor for reference. The light red line is the origin data of PD, and the dark red line is the result of smoothing. We implement three processes in the bath, two heating and one cooling, and the variation trend of the device is consistent with the results of the Pt100 temperature sensor, showing a good temperature response characteristic. The combination of the wavelength scanning and the locking method can enable temperature measurement with a wide temperature range and high resolution.

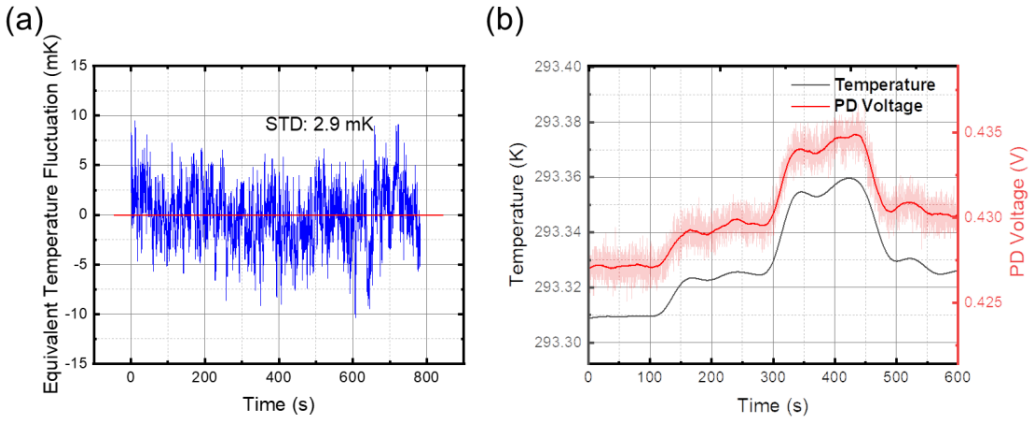

Figure 7. (**a**) The equivalent temperature fluctuation as a function of time, converted from the transmission power stability. (**b**) The temperature response characteristic of the device compared with the Pt100 temperature sensor.

4. Conclusions

In conclusion, a fiber-packaged on-chip silicon thermometer with a WGM ring resonator was demonstrated, and the real-measured temperature range and resolution are 150 K and 2.9 mK, respectively. The device structure, fabrication process, detection system, and measurement performance are presented. Further optimization of the thermometer

resolution can be achieved by reducing the power noise of the laser source and designing the transmission spectrum lineshape to obtain a steeper fringe.

Author Contributions: Conceptualization, J.W. and Y.P.; Data curation, J.W.; Formal analysis, Y.P.; Funding acquisition, Y.P.; Investigation, J.W. and Y.P.; Methodology, J.W., Y.P. and J.G.; Supervision, Y.P., Y.S. and J.Q.; Validation, J.W., J.G., C.Z., Z.Q. and T.X.; Writing—original draft, J.W.; Writing—review & editing, Y.P. All authors have read and agreed to the published version of the manuscript.

Funding: This work was supported by the National Natural Science Foundation of China (No. 62075206).

Institutional Review Board Statement: Not applicable.

Informed Consent Statement: Not applicable.

Data Availability Statement: Data and information developed in this research are available.

Conflicts of Interest: The authors declare no conflict of interest.

References

1. Karvonen, A.; Rintamäki, P.; Jokela, J.; Valtonen, E.T. Increasing water temperature and disease risks in aquatic systems: Climate change increases the risk of some, but not all, diseases. *Int. J. Parasitol.* **2010**, *40*, 1483–1488. [CrossRef] [PubMed]
2. Wunderlich, K.R.A. *On the Temperature in Diseases: A Manual of Medical Thermometry*; New Sydenham Society: London, UK, 1871.
3. Jolesz, F.A. MRI-guided focused ultrasound surgery. *Annu. Rev. Med.* **2009**, *60*, 417–430. [CrossRef] [PubMed]
4. Woo, Y.X.; Nagy, Z.K.; Tan, R.B.H.; Braatz, R.D. Adaptive concentration control of cooling and antisolvent crystallization with laser backscattering measurement. *Cryst. Growth Des.* **2009**, *9*, 182–191. [CrossRef]
5. Knight, C.A.; Ackerly, D.D. An ecological and evolutionary analysis of photosynthetic thermotolerance using the temperature-dependent increase in fluorescence. *Oecologia* **2002**, *130*, 505–514. [CrossRef] [PubMed]
6. Price, R. The Platinum resistance Thermometer. *Platin. Met. Rev.* **1959**, *3*, 78–87.
7. Burns, G.W.; Scroger, M.G. *The Calibration of Thermocouples and Thermocouple Materials*; US Department of Commerce, National Institute of Standards and Technology: Gaithersburg, MD, USA, 1989.
8. Strouse, G.F. Standard platinum resistance thermometer calibrations from the Ar TP to the Ag FP. *NIST Spec. Publ.* **2008**, *250*, 1–66.
9. Berry, R.J. Effect of Pt oxidation on Pt resistance thermometry. *Metrologia* **1980**, *16*, 117. [CrossRef]
10. Berry, R.J. Thermal strain effects in standard platinum resistance thermometers. *Metrologia* **1983**, *19*, 37. [CrossRef]
11. Mihailov, S.J. Fiber Bragg grating sensors for harsh environments. *Sensors* **2012**, *12*, 1898–1918. [CrossRef]
12. Kersey, A.D.; Berkoff, T.A. fiber-optic Bragg-grating differential-temperature sensor. *IEEE Photonics Technol. Lett.* **1992**, *4*, 1183–1185. [CrossRef]
13. Klimov, N.N.; Purdy, T.; Ahmed, Z. On-chip integrated silicon photonic thermometers. *Sens. Transducers* **2015**, *191*, 67.
14. Kim, G.D.; Lee, H.S.; Park, C.H.; Lee, S.S.; Lim, B.T.; Bae, H.K.; Lee, W.G. Silicon photonic temperature sensor employing a ring resonator manufactured using a standard CMOS process. *Opt. Express* **2010**, *18*, 22215–22221. [CrossRef] [PubMed]
15. Xu, H.; Hafezi, M.; Fan, J.; Taylor, J.M.; Strouse, G.F.; Ahmed, Z. Ultra-sensitive chip-based photonic temperature sensor using ring resonator structures. *Opt. Express* **2014**, *22*, 3098–3104. [CrossRef]
16. Weituschat, L.M.; Dickmann, W.; Guimbao, J.; Ramos, D.; Kroker, S.; Postigo, P.A. Photonic and thermal modelling of microrings in silicon, diamond and GaN for temperature sensing. *Nanomaterials* **2020**, *10*, 934. [CrossRef]
17. Zhang, C.; Kang, G.; Xiong, Y.; Xu, T.; Gu, L.; Gan, X.; Pan, Y.; Qu, J. Photonic thermometer with a sub-millikelvin resolution and broad temperature range by waveguide-microring Fano resonance. *Opt. Express* **2020**, *28*, 12599–12608. [CrossRef]
18. Li, B.B.; Wang, Q.Y.; Xiao, Y.F.; Jiang, X.F.; Li, Y.; Xiao, L.; Gong, Q. On chip, high-sensitivity thermal sensor based on high-Q polydimethylsiloxane-coated microresonator. *Appl. Phys. Lett.* **2010**, *96*, 251109. [CrossRef]
19. Dong, C.H.; Sun, F.W.; Zou, C.L.; Ren, X.F.; Guo, G.C.; Han, Z.F. High-Q silica microsphere by poly (methyl methacrylate) coating and modifying. *Appl. Phys. Lett.* **2010**, *96*, 061106. [CrossRef]
20. Klimov, N.; Berger, M.; Ahmed, Z. Towards reproducible ring resonator based temperature sensors. *Sens. Transducers* **2015**, *191*, 63.
21. Klimov, N.; Ahmed, Z. Ring resonator thermometry. In Proceedings of the 2016 IEEE Photonics Conference, Waikoloa, HI, USA, 2–6 October 2016; pp. 99–100.
22. Ahmed, Z.; Cumberland, L.T.; Klimov, N.N.; Pazos, I.M.; Tosh, R.E.; Fitzgerald, R. Assessing radiation hardness of silicon photonic sensors. *Sci. Rep.* **2018**, *8*, 13007. [CrossRef]
23. Kim, H.; Yu, M. Cascaded ring resonator-based temperature sensor with simultaneously enhanced sensitivity and range. *Opt. Express* **2016**, *24*, 9501–9510. [CrossRef] [PubMed]
24. Janz, S.; Cheriton, R.; Xu, D.X.; Densmore, A.; Dedyulin, S.; Todd, A.; Schmid, J.; Cheben, P.; Vachon, M.; Dezfouli, M.; et al. Photonic temperature and wavelength metrology by spectral pattern recognition. *Opt. Express* **2020**, *28*, 17409–17423. [CrossRef]
25. Liao, J.; Yang, L. Optical whispering-gallery mode barcodes for high-precision and wide-range temperature measurements. *Light-Sci. Appl.* **2021**, *10*, 32. [CrossRef]

26. You, M.; Lin, Z.; Li, X.; Liu, J. Chip-scale silicon ring resonators for cryogenic temperature sensing. *J. Lightwave Technol.* **2020**, *38*, 5768–5773. [CrossRef]
27. Tao, J.; Luo, Y.; Wang, L.; Cai, H.; Sun, T.; Song, J.; Liu, H.; Gu, Y. An ultrahigh-accuracy miniature dew point sensor based on an integrated photonics platform. *Sci. Rep.* **2016**, *6*, 29672. [CrossRef]
28. Zhang, C.; Kang, G.G.; Wang, J.; Wan, S.; Dong, C.H.; Pan, Y.J.; Qu, J.F. Photonic thermometer by silicon nitride microring resonator with milli-kelvin self-heating effect. *Measurement* **2022**, *188*, 110494. [CrossRef]
29. Selvaraja, S.K.; Sethi, P. Review on optical waveguides. In *Emerging Waveguide Technology [Internet]*; You, K.Y., Ed.; IntechOpen: London, UK, 2018. Available online: https://www.intechopen.com/chapters/61838 (accessed on 25 March 2022).
30. Taillaert, D.; Bienstman, P.; Baets, R. Compact efficient broadband grating coupler for silicon-on-insulator waveguides. *Opt. Lett.* **2004**, *29*, 2749. [CrossRef]